Journal of Non-Crystalline Solids 498 (2018) 118–124

Contents lists available at ScienceDirect

Journal of Non-Crystalline Solids

journal homepage: www.elsevier.com/locate/jnoncrysol

Amorphous magnesium silicide

Murat Durandurdu

Department of Materials Science & Nanotechnology Engineering, Abdullah Gül University, Kayseri 38080, Turkey

ARTICLE INFO

Keywords:
Intermetallic
Magnesium silicide
Biodegradable
Amorphous

ABSTRACT

A first principles molecular dynamics technique is employed to generate an amorphous magnesium silicide (Mg_2Si) model from its liquid state and its structural, electrical and mechanical features are disclosed for the first time. Si atoms form predominantly the standard square dodecahedron-like and the tri-capped trigonal prism-like configurations while Mg atoms arrange themselves primarily in higher coordinated crystal-like and icosahedral-like polyhedrons. The mean coordination number of Mg and Si is estimated to be ~12.84 and ~8.2, respectively. Si−Si homopolar bonds are also presented in the amorphous network, in contrast to the crystal. Based on our findings, we propose that the amorphous model has a short-range order, quite different than that of the anti-fluorite Mg_2Si crystal but similar to that of metallic glasses. The different local structure of the amorphous state yields distinct electronic and mechanical properties, relative to the crystal. Within the known limitation of DFT-GGA simulations, the amorphous Mg_2Si is found to be semimetal though the anti-fluorite structure is semiconductor. Furthermore, amorphous Mg_2Si is predicted to be less brittle than the crystal structure. Since the potential use of the Mg_2Si crystal as a biodegradable implant material is hindered because of its brittle behavior, here we propose that amorphous or nanoglass forms might eliminate this limitation of Mg_2Si and hence it can serve as an implant material in near future.

1. I. Introduction

Magnesium silicide (Mg_2Si) is an important narrow gap semiconductor (an indirect band gap of about 0.6 eV [1]) of considerable current interest due to its unique physical properties. Mg_2Si is expected to a wide variety of high technological applications. A large Seebeck coefficient, low electrical resistivity, and low thermal conductivity are a few exceptional characteristics of Mg_2Si [2–8], which make it a promising candidate for thermoelectric materials. Since Mg_2Si is an environmentally friendly material [9], it might replace lead-based thermoelectric materials as well. Due to its small band gap, it is also a suitable candidate for an infrared detector [10]. Furthermore, the studies have revealed that Mg_2Si can be used as a new implant material if its brittle character is enhanced [11].

The ground state of Mg_2Si is a face-centered cubic lattice having the anti-fluorite structure ($Fm\bar{3}m$) [12]. Amorphous form of Mg_2Si was also prepared using pulsed laser deposition and rf magnetron sputtering techniques [13]. It was reported that amorphous Mg_2Si could be an anode material in rechargeable lithium batteries since it showed superior cyclability over 200 cycles. Yet to our knowledge, there has not been any attempt to investigate this material in details. In this work, we execute ab initio molecular dynamics (MD) simulations to produce an amorphous Mg_2Si model using the rapid solidification process and expose its local structure, and its electronic and mechanical properties for the first time.

2. Method

Simulations were done using the ab initio density functional theory (DFT) code SIESTA [14]. To estimate the exchange correlation potential, we selected the generalized gradient approximation (GGA) of PBE [15]. To create pseudopotentials, we used the Troullier–Martins method [16]. A numerical basis set with polarization (DZP) was used for the valence electrons. A uniform mesh cutoff of 120 Ry, a finite 3D grid for the calculation of electron density and potentials, was selected for the simulations. One femtosecond was chosen for each MD step. We adopted the isothermal–isobaric ensemble in which temperature and pressure were controlled using velocity scaling and Parrinello-Rahman techniques [17], respectively. No shear deformations were allowed during the thermalization and quenching. The anti-fluorite structure, illustrated in Fig. 1, having 216 atoms (arranged as a 2x3x3 block and 144 Mg and 72 Si atoms) with periodic boundary conditions was used as a starting structure. The initial supercell lengths were L_1 = 12.782 Å and $L_2 = L_3$ = 19.173 Å. This crystalline phase was subjected to 1800 K for 3.0 ps and then the external temperate was reduced to 1400 K in 2.0 ps. At this temperature the configuration was equilibrated for 25 ps. Then the temperature applied was decreased to 300 K in 75 ps. The supercell lengths of the amorphous model at 300 K, given in Fig. 1, were

E-mail address: murat.durandurdu@agu.edu.tr.

https://doi.org/10.1016/j.jnoncrysol.2018.06.019
Received 19 April 2018; Received in revised form 7 June 2018; Accepted 9 June 2018
Available online 15 June 2018

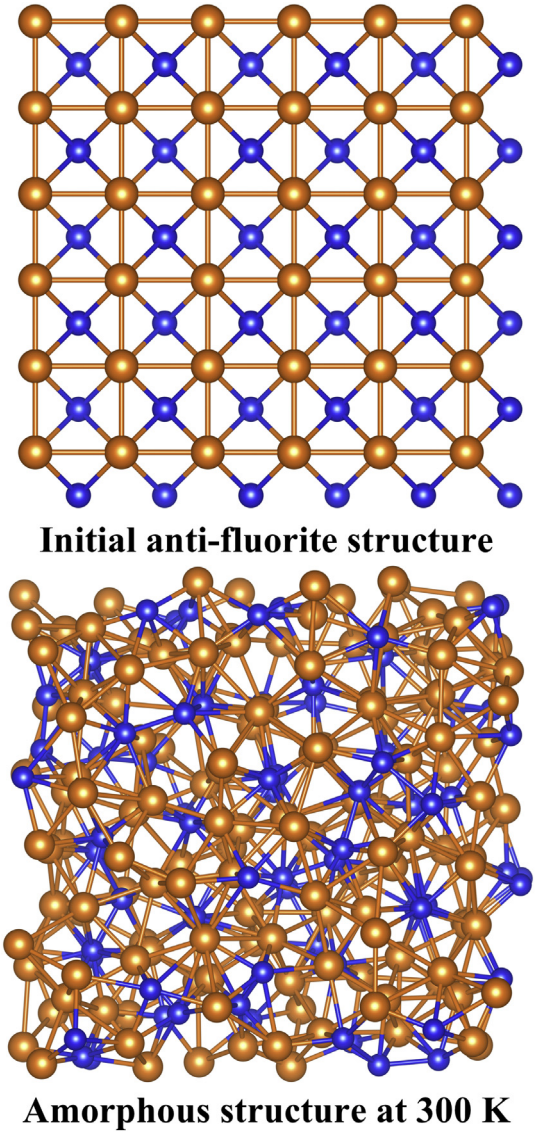

Fig. 1. Ball stick representation of the initial anti-fluorite crystal and the amorphous model at 300 K. Mg and Si atoms are symbolized by large and small spheres, respectively.

L_1 = 10.671386 Å, L_2 = 20.387108 Å and L_3 = 20.972086 Å. Fig. 2 shows the variation of volume per unit formula as a function of temperature. The volume curve decreases gradually and below 700 K it exhibits a change in slope, suggesting the glass-transition temperature (T_g) between 700 and 800 K.

3. Results

3.1. Structural properties

In order to identify the structural features of the amorphous network and compare them with those of the anti-fluorite Mg_2Si phase, we first probe their partial pair distribution functions (PPDFs) and show them in Fig. 3. It can be seen that the peak position of the Mg–Mg, Mg–Si and Si–Si (the second peak) correlations of both structures fairly overlaps each other. Yet the most obvious distinction between these two structures is the presence of Si–Si homopolar bonds as indicated by the peak located at around 2.5 Å in the Si–Si correlation function.

To have a clear description about the short-range order, the partial coordination numbers and the chemical identities around Mg and Si are

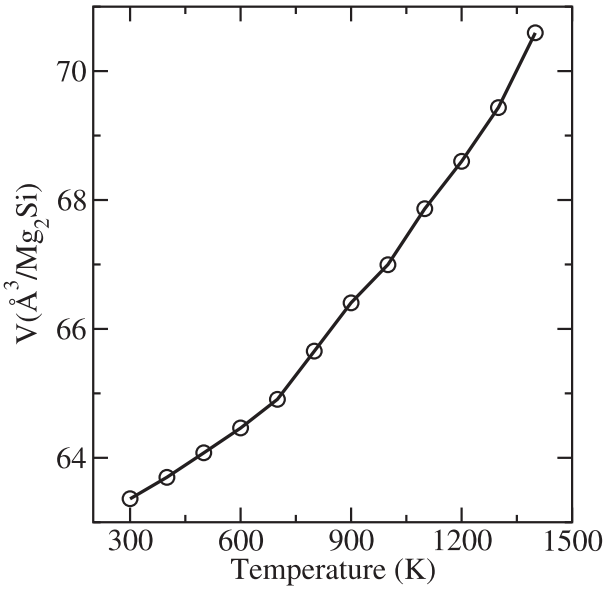

Fig. 2. Variation of volume per unit formula as a function of temperature.

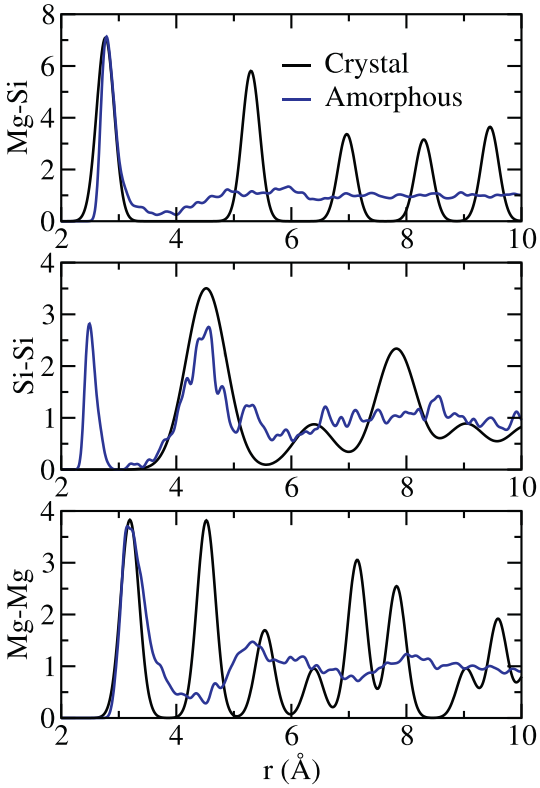

Fig. 3. Partial-pair distribution functions of amorphous and anti-fluorite Mg_2Si. For clarity, the peaks' intensity of the anti-fluorite crystal is reduced.

projected using the Voronoi tessellation technique. The first minimum of the PPDFs is used as the cutoffs that are ~4.0, 3.3, 3.0 Å for Mg–Mg and Mg–Si and Si–Si correlations, respectively. The analysis leads the mean Mg–Mg, Mg–Si, Si–Mg and Si–Si coordination numbers to be ~9, 3.5, 7.1, and 0.86, correspondingly. The average coordination number of Mg and Si atoms is ~12.84 and ~8.2, respectively, which are higher than those of the crystalline phase in which each Mg atom is tenfold coordinated and six of which are Mg atoms ($Mg\text{-}Mg_6Si_4$) while each Si atom is eightfold coordinated and its all neighbors are Mg atoms ($Si\text{–}Mg_8$). We also study the statistical distribution of the clusters

Table 1
Chemical identities around Mg and Si atoms.

Mg		Si	
Mg_9Si_3	15.90%	Mg_7Si_1	27.7%
Mg_9Si_4	14.20%	Mg_8	25.0%
Mg_8Si_4	13.10%	Mg_8Si_1	15.9%
$Mg_{10}Si_3$	9.70%	Mg_6Si_2	8.3%
$Mg_{10}Si_4$	7.90%	Mg_9	8.3%
Mg_9Si_5	6.50%	Mg_7Si_2	4.1%
Mg_7Si_2	4.10%	Mg_5Si_2	4.1%
$Mg_{11}Si_3$	3.80%	Mg_6Si_1	2.0%
Mg_8Si_3	3.40%	Mg_6Si_3	1.3%
$Mg_{11}Si_4$	2.70%	Mg_4Si_2	1.3%
$Mg_{10}Si_5$	2.70%	Mg_7	1.3%
Mg_7Si_4	2.40%		
$Mg_{11}Si_2$	2.00%		
Mg_9Si_2	2.00%		
Mg_8Si_6	1.70%		
$Mg_{12}Si_2$	1.30%		
$Mg_{12}Si_3$	1.30%		
Mg_7Si_5	1.30%		
$Mg_{10}Si_2$	1.30%		
Mg_7Si_3	0.60%		
Mg_{11}	0.60%		

formed in the amorphous network since they can provide additional information about its microstructure. The distribution is summarized in Table 1. In the amorphous structure, the most dominated three clusters around Mg atoms are Mg-Mg_9Si_3 (16%), Mg-Mg_9Si_4 (15%) and Mg-Mg_8Si_4 (13%). We do not find any trace of Mg-Mg_6Si_4 type configuration. For Si atoms, the most common three clusters are Si-Mg_7Si_1 (27%), Si−Mg_8 (25%) and Si-Mg_8Si_1 (15%). So one can see that the environment of only 25% of Si atoms is similar to what has been formed in the crystal.

The Voronoi analysis further allows us to classify the types of the polyhedrons formed in the amorphous structure. A polyhedron is symbolized by a Voronoi index $< n_3, n_4, n_5, n_6, \ldots >$. n_k corresponds to the number of k-edge faces of the polyhedron. The total number of the faces of the Voronoi polyhedron gives the coordination number of the central atom. Fig. 4 illustrates the types and fractions of polyhedra formed around Mg and Si atoms. Si atoms predominantly have two types of polyhedrons, tri-capped trigonal prism < 0 3 6 0 0 > having a fraction of 24% and the standard square dodecahedron < 0 4 4 0 0 > with a frequency of 51%. Mg atoms, on the other hand, present 38 diverse polyhedrons. Nonetheless one can see that the fcc crystal-like < 0 3 6 3 0 > , defective fcc crystal-like < 0 3 6 4 0 > , perfect icosahedron < 0 0 12 0 > and defective or deformed icosahedrons < 0 2 8 1 0 > , < 0 2 8 2 0 > and < 0 1 10 2 0 > are the most favorable ones. Fig. 5 shows some of the most privilege polyhedrons formed in the noncrystalline Mg_2Si.

3.2. Electronic structure

We study the electronic structure of both forms of Mg_2Si. The computed electronic density of states (EDOS) is illustrated in Fig. 6. The Mg_2Si crystal exhibits a semiconductor behavior with small band gap energy while the amorphous phase shows a semi-metallic character. However, it is well known that DFT-GGA simulations underestimate band gap energies and hence the amorphous phase can be semiconductor with a tiny band gap was well. An experimental investigation is really desirable to clarify this matter.

3.3. Mechanical properties

The bulk modulus (K) defining the compressibility of materials can be easily estimated by fitting the energy volume data (calculated using the conjugant gradient variable cell optimization technique) to the

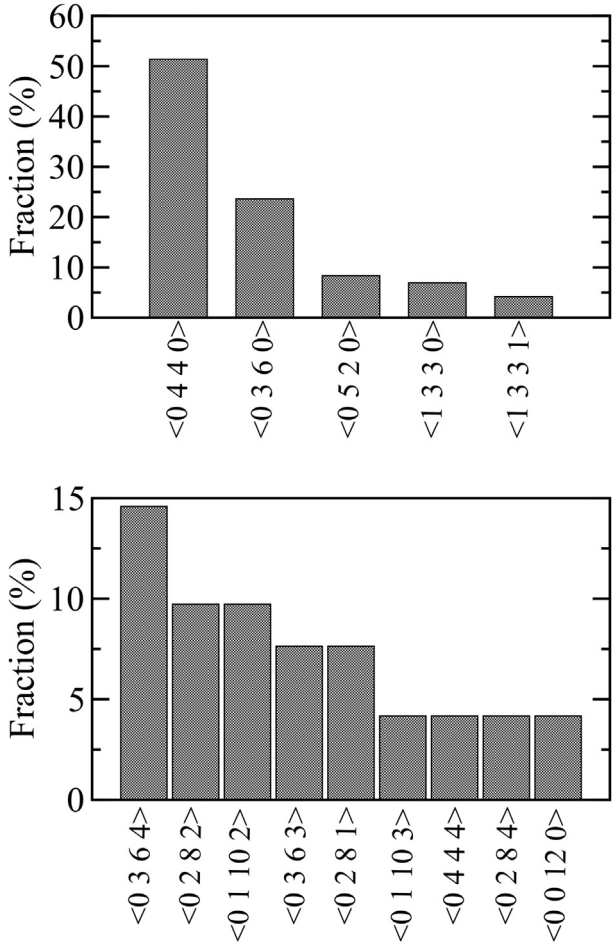

Fig. 4. Fraction of Si-and Mg-centered Voronoi polyhedrons. Polyhedrons having a fraction of less 4% are not shown in the figure.

third-order Birch-Murnaghan equation of states,

$$E(V) = E_o + \frac{9V_OK}{16}\left\{\left[\left(\frac{V_O}{V}\right)^{\frac{2}{3}} - 1\right]^3 K' + \left[\left(\frac{V_O}{V}\right)^{\frac{2}{3}} - 1\right]^2 \left[6 - 4\left(\frac{V_O}{V}\right)^{\frac{2}{3}}\right]\right\}$$

where E (E_o) represents the energy (the zero pressure energy), V (V_o) is the volume (zero pressure volume) and K' is the derivative of K respect to pressure. The energy-volume data for both crystal and amorphous phases are shown in Fig. 7. The relative energy difference between these two phases is ~0.29 eV/Mg_2Si. The equilibrium volume of the crystal is 66.21 Å^3/Mg_2Si, fairly comparable with the previous studies [18–20] (see Table 2). The equilibrium volume of the amorphous model is 62.31 Å^3/ Mg_2Si. The physical origin of such a volume reduction can be attributed to the tendency of Mg atoms to attain higher coordinated configurations in the amorphous network. The K value of the anti-fluorite Mg_2Si crystal is 55.9 GPa, agreeing very well with the other estimations [18–24] (Table 2). For the amorphous phase, the K value is predicted to be 51.6 GPa, comparable with that of the crystal.

In order to evaluate the Poisson's ratio and Young's modulus of the crystal and amorphous states, we study them under uniaxial stresses (compression and tension). The amorphous structure is compressed/tensioned along x-,y- and z-direction, respectively and the change along transverse and axial directions is monitored. The Poisson's ratio of a material exposed to a uniaxial stress is defined as

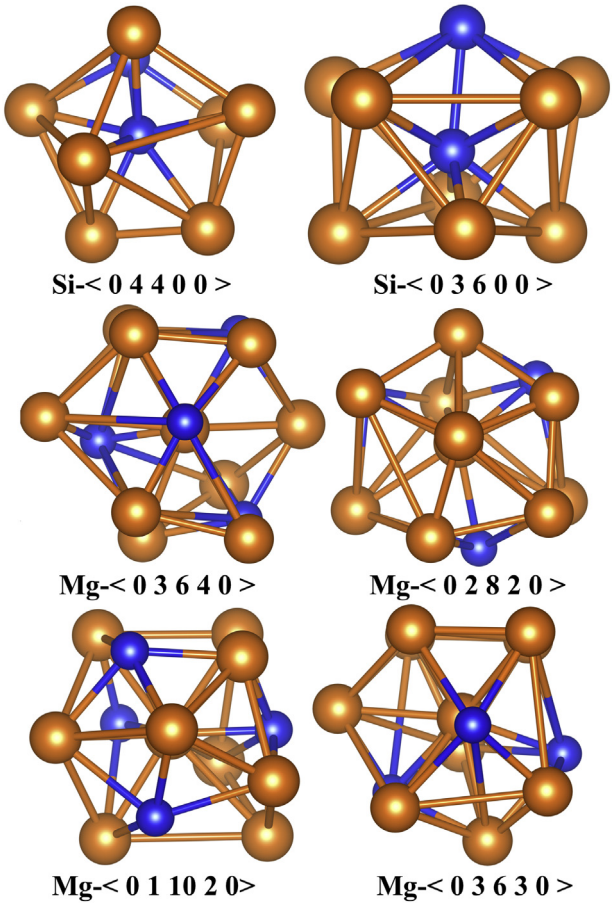

Fig. 5. Some of the most common clusters formed in the noncrystalline Mg_2Si.

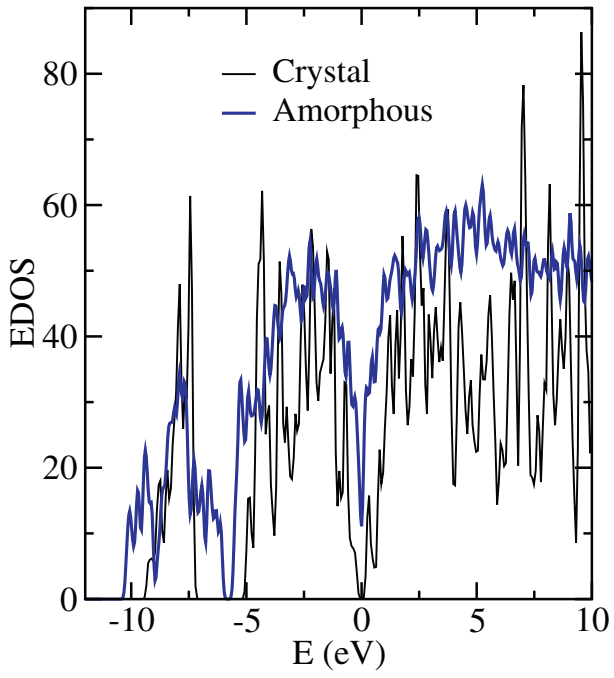

Fig. 6. Electron density of states of amorphous and anti-fluorite Mg_2Si.

$$\nu = -\frac{\varepsilon_{transverse}}{\varepsilon_{axial}}$$

where ε is the strain. The modification of $\varepsilon_{transverse}$ and ε_{axial} for

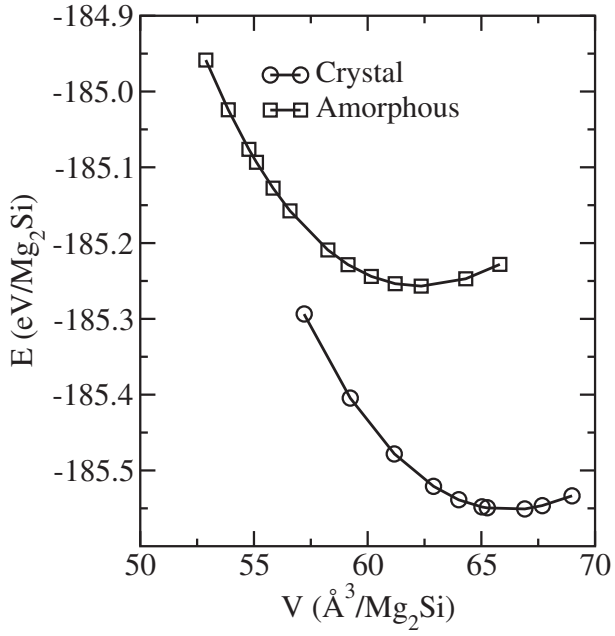

Fig. 7. Energy-volume relation.

amorphous model is given in Fig. 8. We determine the Poisson's ration from the best linear fitting line and have six different values. The mean Poisson's ratio is about 0.3. Because of the cubic symmetry, the crystalline structure is compressed along one-direction and a value of 0.15 for the Poisson's ratio is obtained, which is objectively comparable with the earlier predictions of 0.14–0.19 [21, 23–25, 27, 28]. We should point out here that because of the linear fitting, we surely expect some errors in the Poisson's ratios estimated in the present work. For the glass model, the error is anticipated more as six different values are projected for it. Additionally, under applied stresses, the amorphous model experiences deformations (the simulation box is not orthogonal any more) unlike the crystal. Such minor deformations can produce some errors in the Poisson's ratios computed as well. Subsequently we think that we have some uncertainties in the Poisson's ratio of the glass model.

Since the stress (σ)-strain (ε) relation (see Fig. 9) is known in the simulations, we can simply calculate Young's modulus (E) using the following equation,

$$E = \frac{\sigma_{axial}}{\varepsilon_{axial}}$$

Again from the linear fitting, we obtain three different values. The mean Young's modulus of the glass model is anticipated to be ~61 GPa. For the crystal, it is about 117 GPa and as seen from Table 2, it accords with the previous experimental and theoretical projections of 107–120 GPa [21–28]. Because of the linear fitting, again we might have some errors in the predicted E value but the error is less than what we anticipate in the Poisson's ratio.

Note that the Poisson's ratio can be alternatively calculated using the following relation

$$\nu = \frac{1}{2} - \frac{E}{6K}$$

This equation also yields the Poisson's ratio to be about 0.3, consisting with the direct simulation result.

We compute the shear modulus (μ) using the next definition

$$\mu = \frac{E}{2(1+\nu)}.$$

Shear modulus of the anti-fluorite Mg_2Si is projected to be 51 GPa, which again is in agreement with the earlier estimations of 47–50 GPa

Table 2
The equilibrium parameters of anti-fluorite and amorphous phases. K and K' are bulk modulus and its pressure derivative, V_0 is equilibrium volume per unit formula, ν is Poisson's ratio, E is Young's modulus, μ is shear modulus and H is Vickers hardness.

Structure	a (Å)	V_0 (Å^3)	K(GPa)	K'	ν	E (GPa)	μ (GPa)	H(GPa)	Ref.
$Fm\bar{3}m$	6.43	66.21	55.9	3.46	0.15	117.3	51	14.9[a]	Present
								7.7[b]	Present
	6.29	62.34	57.03	4					[18]
	6.33	63.33	55.64	3.94					[19]
	6.34	63.9	55.35	4					[20]
	6.35		63.36		0.18	119.7	47.1		[21]
	6.35		54.3			107.4	45.9		[22]
	6.29		56.2		0.16	113.5	49.2		[23]
	6.33		51.06		0.14	108.3	46.1		[24]
					0.18	117.2	49.5		[25]
					0.17	117.7	50		[25]
					0.19	116.9	48.9		[25]
								5.4	[25]
								4.8	[25]
								4.3	[26]
					0.17	115.6	49.5		[27]
					0.16	110.9	47.6		[28]
						76		3.96	[30]
Amorphous		62.31	51.6	3.75	0.3	61	24	2.1[a]	Present
								3.6[b]	Present

[a] Chen's equation.
[b] Teter's equation.

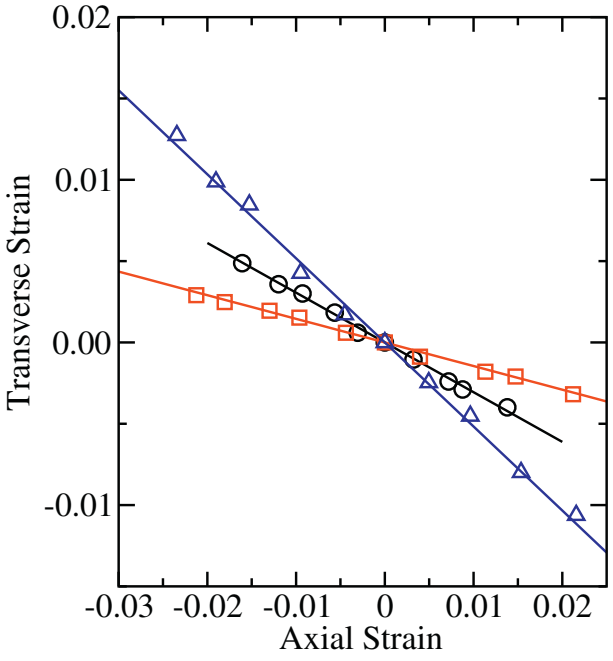

Fig. 8. The variation of $\epsilon_{transfer}$ as a function of ϵ_{axial} for the amorphous model. For clarity, only three fits are shown.

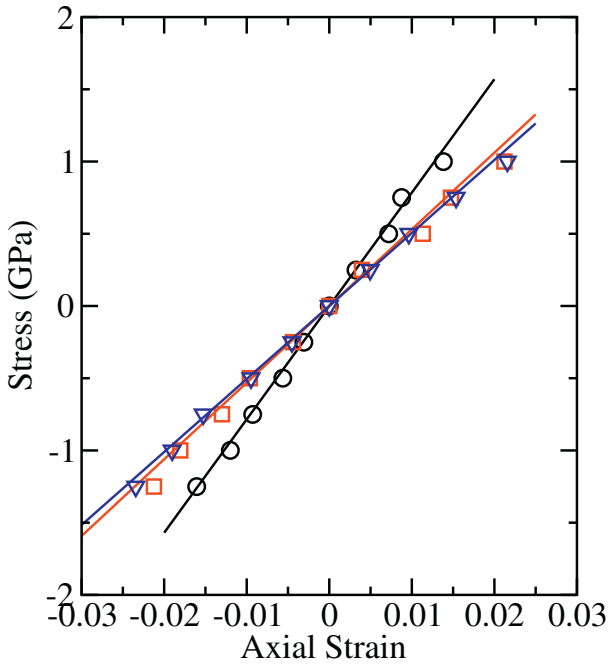

Fig. 9. The stress-strain relation for the amorphous model.

[21–28]. For the amorphous state, the predicted value is about 24 GPa. Using the Chen's equation [29],

$$H = 2\left(\frac{\mu}{n^2}\right)^{0.585} - 3(\text{GPa})$$

where n is the Pugh's ratio ($n = K/\mu$), we can estimate the Vickers hardness of these materials. The hardness is computed to be 14.9 GPa for the crystal, which is about a factor of three larger than the experimental results of 3.96–5.4 GPa [25, 26, 30]. The hardness of the glass configuration is ~2.1 GPa. On the other hand using the Teter's equation [31].

$$H = 0.151\ \mu$$

we calculate H to be 3.6 GPa for the amorphous state and 7.7 GPa for the crystalline Mg_2Si. So one can see that the Teter's equation gives more comparable result with the experiments for the crystal structure.

The ratio μ/K can be used to identify brittle or ductile behavior of materials. For metallic glasses, if μ/K is bigger than 0.41–0.43 (or, equivalently, with $\nu < 0.31$–0.32), then the materials are brittle [32]. Since amorphous Mg_2Si is locally similar to metallic glasses (see below), we use this criterion to identify its behavior. The ratio μ/K is equal to 0.46 and ν is equal to 0.3 for the amorphous state and hence it can be identified as a brittle material, similar to the crystal. Yet it should be noted that both values obtained for the disordered configuration are so close to the critical values and hence it is anticipated to be less brittle than the crystal. The observation might be, perhaps, unsurprising

because Mg atoms in the disordered state have a tendency to form higher coordinated configurations similar to the Mg crystal (hcp has a coordination of 12) that shows a ductile behavior.

4. Discussion

The structural analyses reveal that the local structure of the amorphous Mg_2Si is different than that of the crystal. The general trend of Mg atoms is to attain higher coordinated configurations in the amorphous model similar to what has been reported in Mg based metallic glasses [33, 34]. Additionally the clusters produced around Si atoms are also found to be similar to those reported in the Si based metallic amorphous systems such as PdSi [35]. The different local environment of amorphous Mg_2Si yields diverse electrical and mechanical properties. Perhaps the most remarkable observation is that amorphous Mg_2Si is less brittle than the crystal. The improvement of cyclability of amorphous Mg_2Si might be related to this behavior.

The Mg_2Si crystal is believed to be a good candidate for a biodegradable implant material if its brittle nature is improved [11]. Amorphous Mg_2Si might eliminate this major cumbersome of Mg_2Si. Since its ratio μ/K is so close to the critical value, by slightly changing stoichiometry of Mg_2Si, the brittle-to-ductile transition can be even induced in the amorphous state. Furthermore nanoglasses, “a new kind of noncrystalline materials” [36, 37], present different properties (more ductile, more biocompatible etc.), than corresponding amorphous and crystalline phases [36, 37]. Since the properties of nanoglasses can be controlled by changing their chemical and microstructures and their interfaces can have a new kind of amorphous structure, nanoglass Mg_2Si can be a good candidate to serve as an implant material and/or an anode material in rechargeable lithium batteries as well. Of course, additional studies, especially experimental ones, are really necessary to reveal the correct properties of amorphous and nanoglass Mg_2Si.

5. Conclusions

We use a quantum mechanical MD technique to create an amorphous Mg_2Si model from its melt and reveal its microstructure, and its electrical and mechanical properties for the first time. The average coordination number of Mg and Si in amorphous Mg_2Si are projected to be ~12.84 and ~8.2, correspondingly, which are higher than those of the crystal. Si atoms form mainly the tri-capped trigonal prism-like and the standard square dodecahedron-like configurations, similar to Si based metallic glasses whereas Mg atoms organize themselves in high coordinated crystal-like and icosahedral-like polyhedra as seen in Mg based metallic glasses. Unlike the crystal, the amorphous network has Si−Si homopolar bonds. All these findings reveal that the amorphous model locally differs from the anti-fluorite Mg_2Si crystal. Due to the different local structure, the amorphous configuration has distinct electrical and mechanical properties, compared to the crystal. The anti-fluorite structure is semiconductor whereas amorphous Mg_2Si is semimetal. Perhaps the most interesting finding is that the disordered configuration is less brittle than the crystalline state. Mg_2Si is considered as biodegradable implant material but its brittle nature obstructs its potential uses. We believe that amorphous or nanoglass forms might abolish this restriction of Mg_2Si and thus it can serve as an implant material in near future. We should point out here that all these conclusions are based on a 216 atoms model generated using the melt and quenching technique. Due to the small size of the model, we probably could not capture the medium range order in the model. For larger models, the connectivity of the short-range clusters can be different, which might yield distinct properties than what have been observed in the present study. Furthermore, depending on the preparation procedures, amorphous Mg_2Si with a different local structure and hence the diverse electrical and mechanical properties can be experimentally fabricated. Consequently experimental studies are more desirable to reveal the true behavior of amorphous and nanoglass Mg_2Si.

Acknowledgements

This is work was supported by the Abdullah Gül University Support Foundation. The calculations were run on TÜBİTAK ULAKBİM, High Performance and Grid Computing Center (TRUBA resources).

References

[1] A. Stel La, A.D. Brothers, R.H. Hopkins, W. Lynch, Pressure coefficient of the band gap in Mg_2Si, Mg_2Ge, and Mg_2Sn, Phys. Status Solidi 23 (1967) 697–702.
[2] T. Jun-ichi, K. Hiroyasu, Thermoelectric properties of p-doped Mg_2Si semiconductors, Jpn. J. Appl. Phys. 46 (2007) 3309–3314.
[3] J. Tani, H. Kido, Thermoelectric properties of Bi-doped Mg_2Si semiconductors, Phys. B 364 (2005) 218–224.
[4] T. Jun-ichi, K. Hiroyasu, Thermoelectric properties of Sb-doped Mg_2Si semiconductors, Intermetallics 15 (2007) 1202–1207.
[5] T. Jun-ichi, K. Hiroyasu, J.I. Tani, H. Kido, First-principles and experimental studies of impurity doping into Mg_2Si, Intermetallics 16 (2008) 418–423.
[6] Y. Noda, H. Kon, Y. Furukawa, N. Otsuka, I.A. Nishida, K. Masumoto, Temperature dependence of thermoelectric properties of $Mg_2Si_{0.6}Ge_{0.4}$, Mater. Trans. JIM 33 (1992) 851–855.
[7] W.H. Fan, R.X. Chen, P.D.D. Han, Q.S. Meng, First-principle study of electronic structures of Y-doped Mg_2Si, Mater. Sci. Forum 689 (2011) 102–107.
[8] S.K. Bux, T.Y. Michael, E.S. Toberer, G.J. Snyder, R.B. Kaner, J.P. Fleurial, Mechanochemical synthesis and thermoelectric properties of high quality magnesium silicide, J. Mater. Chem. 21 (2011) 12259–12266.
[9] M. Baleva, G. Zlateva, A. Atanassov, M. Abrashev, E. Goranova, Resonant Raman scattering in ion-beam-synthesized Mg_2Si in a silicon matrix, Phys. Rev. B 72 (2005) 115330–115336.
[10] A. Vantomme, J.E. Mahan, G. Langouche, J.P. Becker, M. Van Aael, K. Temst, C.V. Haesendonck, Thin film growth of semiconducting Mg_2Si by codeposition, Appl. Phys. Lett. 70 (1997) 1086–1088.
[11] K. Hagihara, K. Fujii, A. Matsugaki, T. Nakano, Possibility of Mg-and Ca-based intermetallic compounds as new biodegradable implant materials, Mater. Sci. Eng. C 33 (2013) 4101–4111.
[12] E.A. Owen, G.D. Preston, The atomic structure of two intermetallic compounds, Proc. Phys. Soc. 36 (1924) 341–349.
[13] S.W. Song, K.A. Striebel, X. Song, E.J. Cairns, Amorphous and nanocrystalline Mg_2Si thin-film electrodes, J. Power Sources 119 (2003) 110–112.
[14] P. Ordejón, E. Artacho, J.M. Soler, Self-consistent order-N density-functional calculations for very large systems, Phys. Rev. B 53 (1996) R10441–R10444.
[15] J.P. Perdew, K. Burke, M. Ernzerhof, Generalized gradient approximation made simple, Phys. Rev. Lett. 77 (1996) 3865–3868.
[16] N. Troullier, J.M. Martins, Efficient pseudopotentials for plane-wave calculations, Phys. Rev. B 43 (1991) 993–2006.
[17] M. Parrinello, A. Rahman, Polymorphic transitions in single crystals: a new molecular dynamics method, J. Appl. Phys. 52 (1981) 7182–7190.
[18] J. Hao, B. Zou, P.W. Zhu, C.X. Gao, Y.W. Li, D. Liu, K. Wang, W.W. Lei, Q.L. Cui, G.T. Zou, In situ X-ray observation of phase transitions in under high pressure, Solid State Commun. 149 (2009) 689–692.
[19] F. Yu, J.X. Sun, W. Yang, R.G. Tian, G.F. Ji, A study of the phase transitions, electronic structures and optical properties of under high pressure, Solid State Commun. 150 (2010) 620–624.
[20] J.H. Hao, Z.G. Guo, Q.H. Jin, First principles calculation of structural phase transformation in Mg_2Si at high pressure, Solid State Commun. 150 (2010) 2299–2302.
[21] Q. Chen, Q. Xie, Q.Q. Xiao, J.M. Zhang, The influence of lattice deformation on the elastic properties of Mg_2Si, Sci. China Phys. Mech. Astron. 56 (2013) 701–705.
[22] S. Ganeshan, S.L. Shang, H. Zhang, Y. Wang, M. Mantina, Z.K. Liu, Elastic constants of binary Mg compounds from first-principles calculations, Intermetallics 17 (2009) 313–318.
[23] J. Tania, H. Kido, Lattice dynamics of Mg_2Si and Mg_2Ge compounds from first-principles calculations, Comput. Mater. Sci. 42 (2008) 531–536.
[24] D. Zhou, J. Liu, S. Xu, P. Peng, Thermal stability and elastic properties of Mg 2 X (X = Si, Ge, Sn, Pb) phases from first-principle calculations, Comput. Mater. Sci. 51 (2012) 409–414.
[25] R.D. Schmidt, E.D. Case, J. Giles, J.E. Ni, T.P. Hogan, Room-temperature mechanical properties and slow crack growth behavior of Mg_2Si thermoelectric materials, J. Electron. Mater. 41 (2012) 1210–1216.
[26] G.H. Li, H.S. Gill, R.A. Varin, Magnesium silicide intermetallic alloys, Metall. Trans. A. 24 (1993) 2383–2391.
[27] C. Zhang, P. Han, X. Yan, C. Wang, L. Xia, B. Xu, First-principles study of typical precipitates in creep resistant magnesium alloys, J. Phys. D 42 (2009) 125403–125407.
[28] W.B. Whitten, P.L. Chung, G.C. Danielson, Elastic constants and lattice vibration frequencies of Mg_2Si, J. Phys. Chem. Solids 26 (1965) 49–56.
[29] X.Q. Chen, H. Niu, D. Li, Y. Li, Modeling hardness of polycrystalline materials and bulk metallic glasses, Intermetallics 19 (2011) 1275–1281.
[30] V. Milekhine, M.I. Onsøien, J.K. Solberg, T. Skaland, Mechanical properties of FeSi (ε), FeSi 2 (ζ α) and Mg2Si, Intermetallics 10 (2002) 650–743.
[31] D.M. Teter, Computational alchemy: the search for new superhardmaterials, MRS Bull. 23 (1998) 22–27.
[32] J.J. Lewandowski, W.H. Wang, A.L. Greer, Intrinsic plasticity or brittleness of

metallic glasses, Philos. Mag. Lett. 85 (2005) 77–87.
[33] P. Jóvári, K. Saksl, N. Pryds, B. Lebech, N.P. Bailey, A. Mellergad, R.G. Delaplane, H. Franz, Atomic structure of glassy $Mg_{60}Cu_{30}Y_{10}$ investigated with EXAFS, x-ray and neutron diffraction, and reverse Monte Carlo simulations, Phys. Rev. B 76 (2007) 054208–054216.
[34] D. Liu, S.P. Pan, J.Y. Qin, T.K. Gu, Chemical and topological short-range order evolution of $Mg_{65}Cu_{25}Gd_{10}$ alloy in the process of rapid solidification, J. Appl. Phys. 109 (2011) 093519–093524.
[35] M. Durandurdu, Ab initio modeling of metallic $Pd_{80}Si_{20}$ glass, Comput. Mater. Sci. 65 (2012) 44–47.
[36] H. Gleiter, Nanoglasses: a new kind of noncrystalline, Beilstein J. Nanotechnol. 4 (2013) 517–533.
[37] H. Gleiter, A new kind of noncrystalline material and the way to an age of new technologies? Small 12 (2016) 2225–2233.